



# Evolution of the antibacterial activity and oxidation intermediates during the electrochemical degradation of norfloxacin in a flow cell with a PTFE-doped $\beta$ -PbO<sub>2</sub> anode: Critical comparison to a BDD anode

Isaac Sánchez-Montes<sup>a</sup>, José R. Fuzer Neto<sup>b</sup>, Bianca F. Silva<sup>c</sup>, Adilson J. Silva<sup>b</sup>, José M. Aquino<sup>a,\*</sup>, Romeu C. Rocha-Filho<sup>a,\*\*</sup>

<sup>a</sup> Departamento de Química, Universidade Federal de São Carlos, C.P. 676, 13560-970 São Carlos, SP, Brazil

<sup>b</sup> Departamento de Engenharia Química, Universidade Federal de São Carlos, C.P. 676, 13560-970 São Carlos, SP, Brazil

<sup>c</sup> Instituto de Química de Araraquara, Departamento de Química Analítica, Universidade Estadual Paulista, 14800-900 Araraquara, SP, Brazil

## ARTICLE INFO

### Article history:

Received 26 April 2018

Received in revised form

15 July 2018

Accepted 17 July 2018

Available online 21 July 2018

### Keywords:

Electrooxidation

Boron-doped diamond anode

Hydroxylation reactions

Electrodegradation intermediates

Antibacterial bioassays

## ABSTRACT

The electrochemical degradation of the antibiotic norfloxacin (NOR) was investigated using an electro-deposited polytetrafluoroethylene (PTFE)-doped  $\beta$ -PbO<sub>2</sub> anode; its attained performance was compared to that of a boron-doped diamond (BDD) anode to check out a literature claim of superior performance by the former anode. The PTFE content in the electrodeposition bath was optimized to lead to a significantly extended service life of the  $\beta$ -PbO<sub>2</sub> anode despite its titanium substrate. The NOR degradation electrolyses (100 mg L<sup>-1</sup> NOR in 0.1 mol L<sup>-1</sup> Na<sub>2</sub>SO<sub>4</sub>) were carried out in a filter-press flow cell (flow rate of 420 L h<sup>-1</sup>) using the following optimized conditions: no pH control, current density of 10 mA cm<sup>-2</sup>, and 40 °C. The electrooxidation process performance under these conditions was assessed through the evolution of the attained removals of NOR, total organic carbon (TOC), and antibacterial activity against *Escherichia coli*; the evolution of oxidation intermediates (aromatic compounds and carboxylic acids) was also assessed. In spite of the complete oxidation of NOR, the TOC removal attained with the PTFE-doped  $\beta$ -PbO<sub>2</sub> anode was relatively low (70% after 12 h, compared to 90% after only 5 h for a Si/BDD anode). As a consequence of this inferior performance comparatively to that of a BDD anode, a higher number of aromatic intermediates was detected; these intermediates seemed to still present antibacterial activity against *Escherichia coli*, which lasted even after all NOR was oxidized, contrary to the case of the electrooxidation with a BDD anode. The performance of the PTFE-doped  $\beta$ -PbO<sub>2</sub> anode was not superior to that of a BDD anode, i.e. the doping of the  $\beta$ -PbO<sub>2</sub> film with PTFE, making it hydrophobic, does not change the oxidation power of the anode despite increasing its service life.

© 2018 Elsevier Ltd. All rights reserved.

## 1. Introduction

Nowadays, water contamination by organic compounds (organics), such as antibiotics, pesticides and personal care products, is one of the main concerns of our society [1]. In this context, the inadequate use, management, and disposal of antibiotics may lead to the contamination of water bodies and consequent chronic toxic effects in humans, as well as to the enhancement of antibiotic resistance [2,3]. Furthermore, as noted in the literature [4], organics

(particularly antibiotics [5–7]) are unlikely to be completely eliminated by conventional municipal treatment plants because of their complex chemical structures and distinct physicochemical properties. All these environmental concerns are reflected in the increasing number of papers on the synthesis of new materials for use in organics degradation (e.g. Refs. [8–10]). Despite all these efforts, care must be taken to choose and use suitable treatment methods [11] that are also compatible with financial constraints and environmental regulations [12].

Among the available methods, electrochemical processes and their coupled variations [13,14] have been investigated to treat solutions/effluents contaminated with organics, aiming at mineralizing them to CO<sub>2</sub>; however, this has been successfully achieved (i.e. with high removal rates and current efficiencies, with no

\* Corresponding author.

\*\* Corresponding author.

E-mail addresses: [jmaquino@ufscar.br](mailto:jmaquino@ufscar.br) (J.M. Aquino), [romeu@ufscar.br](mailto:romeu@ufscar.br) (R.C. Rocha-Filho).

formation of toxic by-products) mostly with boron-doped diamond (BDD) anodes [14,15] due to their high oxidation power, a consequence of the reactivity of the quasi-free hydroxyl radicals ( $\text{HO}^\bullet$ ) formed on their surface [16,17]. Sb-doped  $\text{SnO}_2$  and  $\beta\text{-PbO}_2$  (commonly supported on a Ti substrate) are anode materials of medium oxidation power that can potentially be used in organics degradation [17]. However, as noted in the literature (e.g. Refs. [18,19]), film instability associated with the passivation of the Ti substrate as well as poor removal rates [20] and low current efficiencies are still common problems with such anodes. Some of the strategies to overcome these difficulties have been focused on the organic and inorganic doping of those metal oxides. In this sense,  $\beta\text{-PbO}_2$  is one of the most investigated anode materials concerning both inorganic [10,19–22] and organic [23,24] doping, modification of the Ti substrate to avoid migration of the ion  $\text{O}^{2-}$  (e.g. using Pt [25,26] or oxide [20,24,27] coatings, some of them nanostructured [10,28]), usage of 3D substrates [29–31] or graphene interlayers [32], and changes in the  $\beta$ -phase morphology [33] to increase the film stability and the mineralization efficiency in the organics degradation. The use of transition metals as inorganic dopants of  $\beta\text{-PbO}_2$  has led to an increase in its electrocatalytic power for organics oxidation [10,20,21], whereas the use of fluoride ion-based electrolytes [34] and fluorine-based polymers (polyvinylidene difluoride – PVDF [23,24] or polytetrafluoroethylene – PTFE [35]) in the electrodeposition bath have led to  $\beta\text{-PbO}_2$  films with longer-lasting stability (as inferred from service life determinations). In addition, it is often reported that the amount of  $\text{HO}^\bullet$  produced on the surface of PTFE- and PVDF-doped  $\beta\text{-PbO}_2$  anodes is high or, in some cases, higher than that on the surface of BDD anodes [35]. However, the reported oxidation and mineralization removal rates are still below the excellent values commonly reported for BDD anodes [36], with one exception [35]. On the other hand, very little is known about the oxidation intermediates of the electrochemical degradation of organics on PTFE-doped  $\beta\text{-PbO}_2$  anodes; less yet is known about the toxicity of these intermediates.

Considering the environmental problems caused by antibiotic contamination and the reduced number of papers reporting investigations of the degradation intermediates (and their potential toxic effects on microorganisms) generated when PTFE-doped  $\beta\text{-PbO}_2$  anodes are used, the aim of this work is to obtain and characterize different PTFE-doped  $\beta\text{-PbO}_2$  anodes, as well as to use the best such anode (that of longest service life) in the electrochemical degradation of norfloxacin (NOR), a second-generation fluoroquinolone antibiotic (the attained performances will be compared to those recently reported for BDD anodes [37]). The main idea is to reproduce the obtention of hydrophobic  $\beta\text{-PbO}_2$  films and comparatively investigate whether their oxidation capability is indeed greater than that of BDD films, as claimed by Zhao et al. [35]. This will be carried out by comparing the attained removals of NOR and total organic carbon (TOC), which yield information on the oxidation and mineralization efficiency, respectively; additionally, these removals will be compared to those estimated through a theoretical model based on a process purely controlled by mass transport. Furthermore, initial (aromatic compounds) and terminal (short-chain carboxylic acids) oxidation intermediates will also be compared, as well as the antibacterial activity of the NOR electrolyzed solution against *Escherichia coli* (*E. coli*), assessed after different electrolysis times.

## 2. Experimental

### 2.1. Chemicals

All chemicals, including NOR (99.9%, Vita Nova),  $\text{Pb}(\text{NO}_3)_2$  (a.r., Acros),  $\text{HNO}_3$  (69–70%, JT Baker),  $\text{Na}_2\text{SO}_4$  (a.r., Qhemis),  $\text{KH}_2\text{PO}_4$

(a.r., Sigma Aldrich),  $\text{H}_3\text{PO}_4$  (85%, Mallinckrodt),  $\text{Na}_2\text{S}_2\text{O}_8$  (a.r., Sigma Aldrich), carboxylic acids (a.r., Sigma Aldrich), methanol (HPLC grade, JT Baker) and the polytetrafluoroethylene dispersion – PTFE (60%, DuPont), were used as received. Deionized water (Millipore Milli-Q, resistivity  $\geq 18.2 \text{ M}\Omega \text{ cm}$ ) was used throughout.

### 2.2. PTFE-doped $\beta\text{-PbO}_2$ film preparation and characterization

The PTFE-doped  $\beta\text{-PbO}_2$  films were anodically electrodeposited on both sides of a Ti substrate that was previously sandblasted using 60–70  $\mu\text{m}$  glass microspheres and then cleaned for 30 min in an ultrasonic bath containing 2-propanol. The electrodeposition baths were obtained by adding different volumes of the PTFE dispersion to a volume of an aqueous  $0.1 \text{ mol L}^{-1} \text{ Pb}(\text{NO}_3)_2 + 0.1 \text{ mol L}^{-1} \text{ HNO}_3$  solution; the actual volumetric ratios of the PTFE dispersion to the aqueous solution ( $V_{\text{RPTFE}}$ ) were 2, 4, 6, 8, and  $10 \text{ mL L}^{-1}$ . The electrodepositions were carried out (using two AISI-304 stainless steel plates as counter electrodes) at  $5 \text{ mA cm}^{-2}$  and  $65^\circ \text{C}$  for the time necessary to attain  $50 \text{ mg cm}^{-2}$  of  $\text{PbO}_2$  film (assuming 100% faradaic efficiency), according to a previous work [25]. Immediately after each electrodeposition, the obtained electrode (hereinafter referred as Ti/ $\beta\text{-PbO}_2$ ,PTFE) was transferred to a vessel containing deionized water at  $65^\circ \text{C}$ , which was then slowly cooled down to room temperature; this procedure minimized the possibility of formation of cracks in the PTFE-doped  $\beta\text{-PbO}_2$  films.

The obtained electrodes were analyzed by: i) field emission scanning electron microscopy – FESEM (FEI inspect F50), for morphological characterization; ii) X-ray diffraction (RU200B Rigaku Rotaflex diffractometer, from  $20^\circ$  to  $80^\circ$ ,  $\text{CuK}\alpha$   $1.5406 \text{ \AA}$ ), to check whether the desired  $\beta$ -phase crystalline structure was obtained; iii) contact angle measurements, to check whether the co-deposition of PTFE led to hydrophobic films; iv) cyclic voltammetry (CV), to characterize the  $\beta\text{-PbO}_2$  oxidation and reduction peaks; v) chronopotentiometry (at  $500 \text{ mA cm}^{-2}$ ), for service life (SL) estimation. The CV measurements ( $20 \text{ mV s}^{-1}$ ) were performed in  $0.5 \text{ mol L}^{-1} \text{ H}_2\text{SO}_4$  at  $25^\circ \text{C}$  using a conventional three-electrode cell, with a Pt foil counter electrode and an Ag/AgCl ( $3 \text{ mol L}^{-1} \text{ KCl}$ ) reference electrode. The SL estimations were performed in  $0.5 \text{ mol L}^{-1} \text{ H}_2\text{SO}_4$  at  $65^\circ \text{C}$  using a two-electrode cell, with a Pt foil counter electrode. All the electrochemical measurements were carried out using a PGSTAT 20 Autolab potentiostat/galvanostat controlled by the GPES software.

### 2.3. CV measurements

For the Ti/ $\beta\text{-PbO}_2$ ,PTFE electrode (exposed area:  $0.73 \text{ cm}^2$ ) of optimized composition (longest SL), CV measurements ( $20 \text{ mV s}^{-1}$ ) of a  $0.1 \text{ mol L}^{-1} \text{ Na}_2\text{SO}_4$  solution in the presence or absence of  $100 \text{ mg L}^{-1} \text{ NOR}$  (at  $25^\circ \text{C}$ ) were performed using the previously mentioned three-electrode cell.

### 2.4. Electrochemical degradation experiments and analyses

The NOR electrochemical degradation experiments were carried out in a one-compartment filter-press flow reactor, with the double-sided Ti/ $\beta\text{-PbO}_2$ ,PTFE anode (exposed area:  $2.8 \text{ cm} \times 4.2 \text{ cm}$ , each side) of optimized composition (longest SL) and two AISI 304 stainless steel plates cathodes, as described elsewhere [38] – see Fig. SC–1 in the supplementary content file. In these electrolyses,  $0.5 \text{ L}$  of an aqueous  $100 \text{ mg L}^{-1} \text{ NOR}$  solution in  $0.1 \text{ mol L}^{-1} \text{ Na}_2\text{SO}_4$  was used. The effect of the following variables (and respective ranges) was investigated: pH (3, 7, 10, and no pH control), current density ( $10$ ,  $20$ , and  $30 \text{ mA cm}^{-2}$ ), and temperature ( $10$ ,  $25$ , and  $40^\circ \text{C}$ ). The solution pH was continuously monitored and, if

necessary, kept constant at the desired value by addition of a concentrated H<sub>2</sub>SO<sub>4</sub> or NaOH solution. The volumetric flow rate ( $q_v$ ) and electrolysis time were kept fixed at 420 L h<sup>-1</sup> (corresponding to a flow velocity of 0.29 m s<sup>-1</sup>) and 300 min, respectively. To assure that the anode surface was initially clean (no organics adsorbed), before each degradation electrolysis the anode was electrochemically pretreated in 0.1 mol L<sup>-1</sup> Na<sub>2</sub>SO<sub>4</sub> by applying 20 mA cm<sup>-2</sup> for 15 min.

The possible release of Pb<sup>2+</sup> ions from the anode surface during the electrochemical degradation experiments was checked at the end of the electrolysis by atomic absorption spectroscopy (AAS) analyses of the electrolyzed solutions.

The [NOR] evolution during the electrolyses was monitored by HPLC using a core shell C-18 reversed phase column as the stationary phase (Phenomenex: 150 mm × 4.6 mm, 5 μm particle, 100 Å) and a mixture of aqueous 10 mmol L<sup>-1</sup> KH<sub>2</sub>PO<sub>4</sub> at pH 3 (eluent A) and methanol (eluent B) as the mobile phase in a gradient elution mode: from 10% of eluent B to 90% in 10 min and then back to 10% of eluent B in 3 min. LC-MS/MS determinations of the initial intermediate compounds were carried out every 1 h until 8 h of electrolysis. All procedures concerning extraction, preparation, and analyses of the electrolyzed samples by LC-MS/MS were performed as previously reported [37]. For analysis purposes, the removal of NOR during the electrolyses will be viewed through its remaining fraction, i.e. as  $x_{\text{NOR}}^{\text{rem}} = [\text{NOR}]_t / [\text{NOR}]_0$ , where [NOR]<sub>t</sub> and [NOR]<sub>0</sub> are the values at time  $t$  and before the beginning of the given electrolysis, respectively.

The extent of mineralization during the electrolyses was monitored by determinations of the total organic carbon concentration ([TOC]) every 1 h, proceeding as previously reported [37]. For analysis purposes, the removal of TOC during the electrolyses will be viewed through its remaining fraction, i.e. as  $x_{\text{TOC}}^{\text{rem}} = [\text{TOC}]_t / [\text{TOC}]_0$ , where [TOC]<sub>t</sub> and [TOC]<sub>0</sub> are the values at time  $t$  and before the beginning of the given electrolysis, respectively.

The antibacterial activity tests of electrolyzed and initial solution samples were carried out using *E. coli* bacteria, as previously described [37]. The antibacterial activity of the samples was assessed through the inhibition index ( $I$ ), calculated according to [39]:

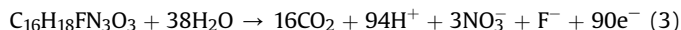
$$I = \left( \frac{A_0 - A}{A_0} \right) \quad (1)$$

where  $A_0$  and  $A$  are the absorbance in the absence (negative control samples) and presence (samples from all the investigated electrolysis times) of NOR, respectively.

The mineralization current efficiency (MCE) was calculated according to [40]:

$$\text{MCE} = \frac{\delta[\text{TOC}]_t n F V}{4.32 \times 10^7 m I t} \quad (2)$$

where  $\delta[\text{TOC}]_t$  is the measured removal of [TOC] (mg L<sup>-1</sup>) after a certain time  $t$  (h),  $n$  the number of exchanged electrons (90 – see equation (3)) considering that the applied electric charge was consumed solely in the mineralization process,  $F$  the Faraday constant (96485 C mol<sup>-1</sup>),  $V$  the sample solution volume (L),  $4.32 \times 10^7$  a conversion factor (i.e. 12000 mg mol<sup>-1</sup> × 3600 s h<sup>-1</sup>),  $m$  the number of carbon atoms in the NOR molecule, and  $I$  the applied electric current (A).



The extent of electrochemical combustion ( $\varphi$ ) [41] of the removed NOR was calculated as the ratio between the fractions of

TOC and NOR removed after a given time of electrolysis under the optimized conditions:

$$\varphi = \frac{1 - x_{\text{TOC}}^{\text{rem}}}{1 - x_{\text{NOR}}^{\text{rem}}} \quad (4)$$

As previously noted [37], the value of  $\varphi$  gives an indication of the extent of conversion of NOR to CO<sub>2</sub>.

Finally, the energy consumption per unit mass ( $w$ ) for the removal of TOC at a given electrolysis time  $t$  (h) was calculated according to [40]:

$$w = \left( \frac{U I t}{\delta[\text{TOC}]_t V} \right) \quad (5)$$

where  $U$  is the cell voltage (V),  $I$  the applied electric current (A), and  $V$  the solution volume (L).

### 3. Results and discussion

#### 3.1. Characterization of the Ti/β-PbO<sub>2</sub>/PTFE electrodes

To investigate the effect of PTFE doping on the properties of the Ti/β-PbO<sub>2</sub>/PTFE electrodes, they were prepared using electrodeposition baths with different  $V_{\text{RPTFE}}$  values. FESEM micrographs of the thus prepared electrodes are shown in Fig. 1. Firstly, it is interesting to note that the characteristic crystallites of the β phase were grown in all conditions and without refinement. When F<sup>-</sup> ions are used in the electrodeposition bath [34], crystallite refinement is commonly observed due to the substitution of O<sup>2-</sup> ions by F<sup>-</sup> ions in defect positions of the β-phase lattice. Further analyzing the FESEM micrographs, a different phase (possibly agglomerated PTFE particles) can be clearly observed between the electrodeposited crystallites only for the electrode obtained using  $V_{\text{RPTFE}} = 2 \text{ mL L}^{-1}$  (see Fig. 1a). This phase, which is present to different extents in all electrodes independently of the value of  $V_{\text{RPTFE}}$  used in the electrodeposition bath, can be better seen under higher magnification in Fig. 1f (similar results were observed by Li et al. [23]); when β-PbO<sub>2</sub> is electrodeposited in the absence of the PTFE dispersion, the borders between grains are sharply defined (see Fig. 1Sa in the supplementary material file of Ref. [25]), instead of being blurred as is the case in the micrographs shown in Fig. 1. Consequently, it can be inferred that clusters of the PTFE dispersion are being co-deposited with the β-PbO<sub>2</sub> crystallites. This inference is corroborated by the fact that agglomerated white particles become apparent when the β-PbO<sub>2</sub> film is dissolved and by the results obtained in water contact angle measurements, when values of ~150° were obtained for all investigated samples – see Fig. SC-2 in the supplementary content file; for comparison purposes, this figure also includes the water contact angle (of ~80°) on a β-PbO<sub>2</sub> film electrodeposited in the presence of sodium dodecyl sulfate (SDS) [25], an electrodeposition additive that has been extensively investigated by our group (see e.g. Ref. [42]). A faradaic efficiency of about 96% was estimated for the β-PbO<sub>2</sub> electrodepositions independently of the  $V_{\text{RPTFE}}$  used in the electrodeposition baths; furthermore, uniform deposition over the Ti substrate was always attained, i.e. no substrate remained exposed.

Next, the prepared Ti/β-PbO<sub>2</sub>/PTFE electrodes were characterized by X-ray diffraction – see Fig. 2. No significant differences can be observed among the diffractograms and all diffraction peaks could be ascribed to the desired β phase (by indexing to the JCPDS card no. 41-1492). This result, also reported for other PbO<sub>2</sub> films deposited in the presence of fluorine-based polymers in the electrodeposition bath [23,35], was expected because the conditions used during the electrodeposition process (hot acidic solutions)

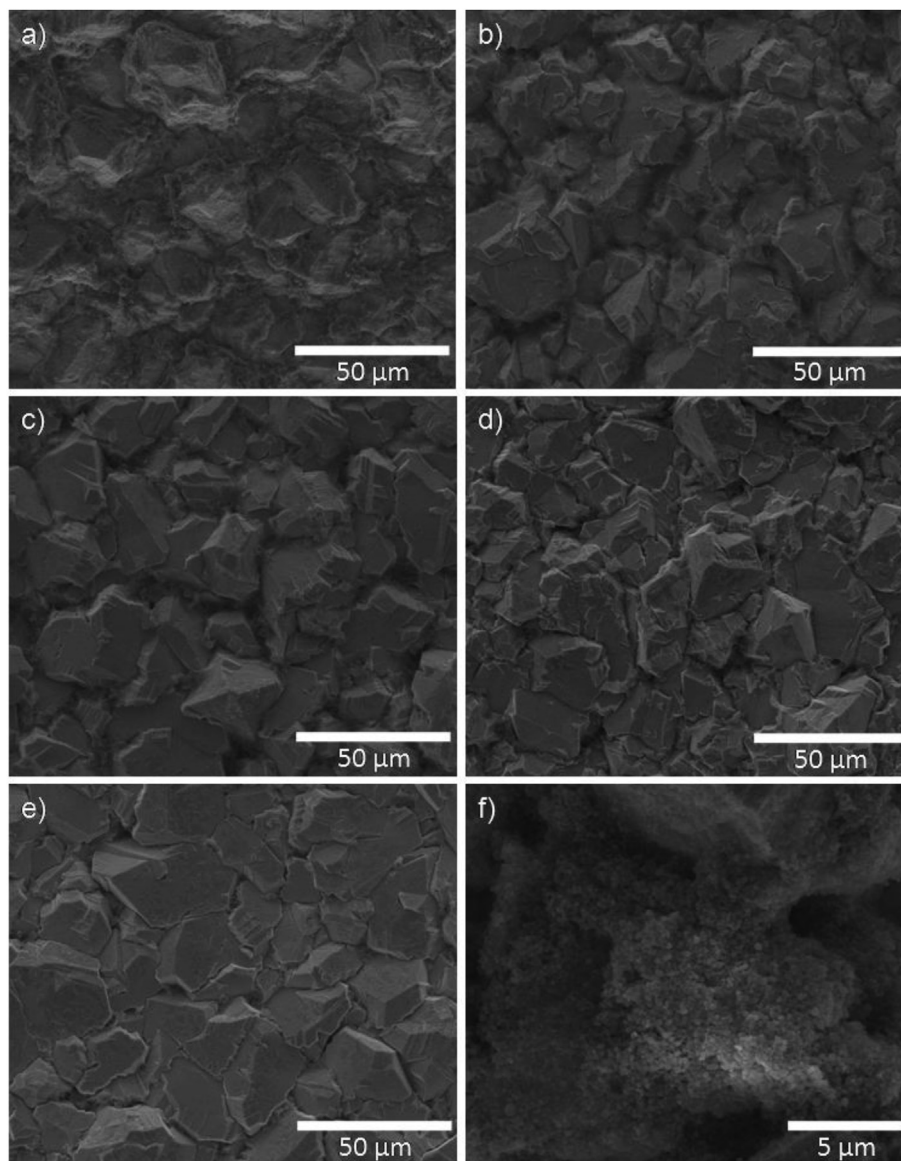


**Fig. 1.** FESEM micrographs of the Ti/ $\beta$ -PbO<sub>2</sub>,PTFE electrodes obtained using electrodeposition baths with different  $V_{R_{PTFE}}$  values: **a)** and **f)** 2 mL L<sup>-1</sup>; **b)** 4 mL L<sup>-1</sup>; **c)** 6 mL L<sup>-1</sup>; **d)** 8 mL L<sup>-1</sup>; **e)** 10 mL L<sup>-1</sup>.

favor the formation of the  $\beta$  phase.

Cyclic voltammetric profiles of the different Ti/ $\beta$ -PbO<sub>2</sub>,PTFE electrodes were obtained in 0.5 mol L<sup>-1</sup> H<sub>2</sub>SO<sub>4</sub> – see Fig. 3 (data for the 5th cycle); for comparison purposes, data are also shown for a  $\beta$ -PbO<sub>2</sub> electrode electrodeposited in the presence of SDS (no PTFE present) [25,42]. As can be seen in this figure, the characteristic peaks for the reduction of Pb(IV) to Pb(II) (at ~1.2 V) [43] and for its re-oxidation to Pb(IV) (at ~1.8 V) were observed for all tested electrodes. On the other hand, as can be inferred by comparing the cathodic and anodic peaks in the voltammograms, the PbO phase formed during the reduction process was not completely converted back to the PbO<sub>2</sub> phase during the oxidation process; thus, these electrodes were not used in any additional studies, being simply discarded.

The final characterization of the different Ti/ $\beta$ -PbO<sub>2</sub>,PTFE electrodes was the estimation of their SL; again, for comparison purposes, this was also done for a Ti/ $\beta$ -PbO<sub>2</sub> anode electrodeposited in the presence of SDS (no PTFE present) [25,42]. The corresponding chronopotentiometric curves are depicted in Fig. 4. Clearly, the SL of

the PTFE-doped  $\beta$ -PbO<sub>2</sub> films is significantly longer, i.e. electrode passivation (characterized by the sharp rise in the cell voltage) occurs after times that are up to fourfold longer than the one for the  $\beta$ -PbO<sub>2</sub> film grown in the presence of SDS only. This excellent performance could be due to the hydrophobic nature of the  $\beta$ -PbO<sub>2</sub>,PTFE films, which lead to a low penetration of the solution through the film, as well as a lower migration rate of O<sup>2-</sup> ions toward the Ti substrate, as discussed by Chen et al. [44]. Among the distinct Ti/ $\beta$ -PbO<sub>2</sub>,PTFE anodes, the one prepared using  $V_{R_{PTFE}} = 6$  mL L<sup>-1</sup> presented the longest SL (860 min) under accelerated conditions; thus, the investigation of the electrochemical degradation of NOR was carried out using this anode. The following relation between SL and the applied electric current density ( $j$ ) has been proposed [44]:

$$SL \propto \frac{1}{jn} \quad (6)$$

where  $n$  ranges from 1.4 to 2.0. Thus, assuming the mean value (1.7)



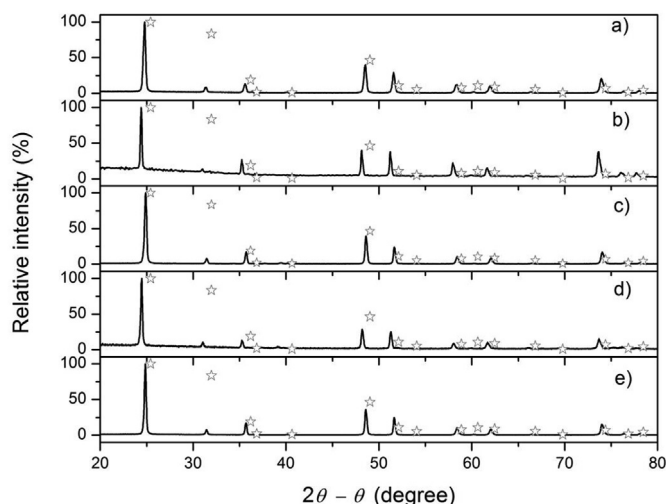


**Fig. 2.** X-ray diffractograms of the Ti/β-PbO<sub>2</sub>/PTFE electrodes obtained using electrodeposition baths with different  $VR_{PTFE}$  values: **a)** 2 mL L<sup>-1</sup>; **b)** 4 mL L<sup>-1</sup>; **c)** 6 mL L<sup>-1</sup>; **d)** 8 mL L<sup>-1</sup>; **e)** 10 mL L<sup>-1</sup>. The symbols refer to the relative intensities of the β-PbO<sub>2</sub> phase according to the JCPDS card no. 41-1492.

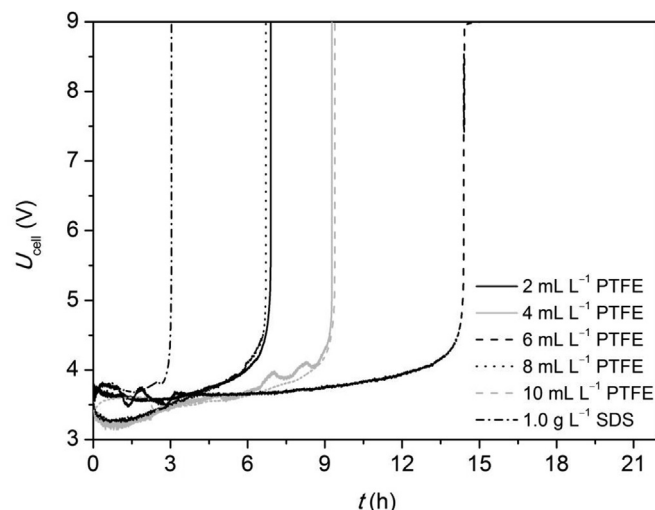


**Fig. 4.** Chronopotentiometric curves (at 500 mA cm<sup>-2</sup>) for Ti/β-PbO<sub>2</sub>/PTFE electrodes obtained using electrodeposition baths with different  $VR_{PTFE}$  values (indicated in the figure). The chronopotentiometric curve depicted as (-.-.-.-) refers to a Ti/β-PbO<sub>2</sub> electrode obtained using an electrodeposition bath with sodium dodecyl sulfate (SDS) as additive (no PTFE present). Electrolyte solution: 0.5 mol L<sup>-1</sup> H<sub>2</sub>SO<sub>4</sub> at 65 °C.

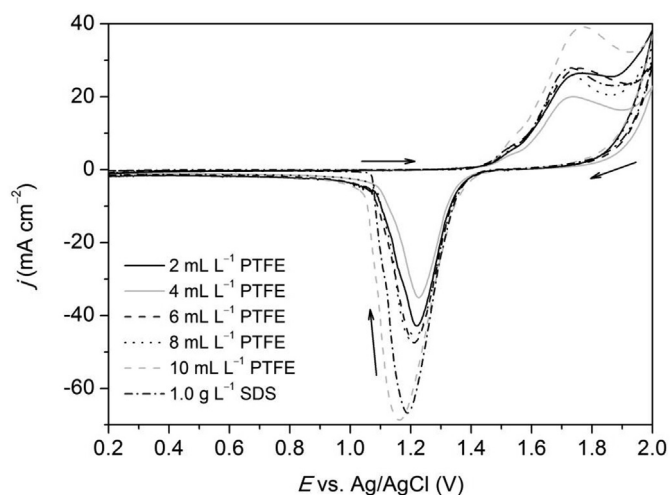


**Fig. 3.** Cyclic voltammograms (5th cycle at 20 mV s<sup>-1</sup>) for Ti/β-PbO<sub>2</sub>/PTFE electrodes obtained using electrodeposition baths with different  $VR_{PTFE}$  values (indicated in the figure). The voltammogram depicted as (-.-.-.-) refers to a Ti/β-PbO<sub>2</sub> electrode obtained using an electrodeposition bath with sodium dodecyl sulfate (SDS) as additive (no PTFE present). Electrolyte solution: 0.5 mol L<sup>-1</sup> H<sub>2</sub>SO<sub>4</sub> at 25 °C. The arrows indicate scan directions.

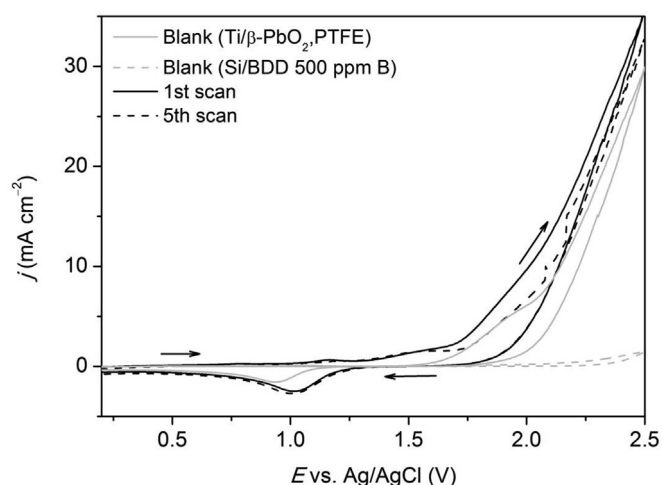


**Fig. 5.** Cyclic voltammograms (20 mV s<sup>-1</sup>, 1st and 5th scans – indicated in the figure) obtained for 100 mg L<sup>-1</sup> NOR in 0.1 mol L<sup>-1</sup> Na<sub>2</sub>SO<sub>4</sub> using the Ti/β-PbO<sub>2</sub>/PTFE electrode prepared with  $VR_{PTFE} = 6$  mL L<sup>-1</sup>. Blank cyclic voltammograms (indicated in the figure) were obtained in a 0.1 mol L<sup>-1</sup> Na<sub>2</sub>SO<sub>4</sub> solution using the previously mentioned electrode or a boron-doped diamond (at 500 ppm of B) electrode. The arrows indicate scan directions.

for n, it is possible to estimate an SL value of ~5 months for this Ti/β-PbO<sub>2</sub>/PTFE anode used in acidic solutions (at 65 °C) at an applied electric current density of ~20 mA cm<sup>-2</sup>. At room temperature, it is reasonable to expect an even longer SL.

### 3.2. Voltammetric characterization of NOR

**Fig. 5** shows cyclic voltammograms (1st and 5th scans) obtained for a 100 mg L<sup>-1</sup> NOR solution (in 0.1 mol L<sup>-1</sup> Na<sub>2</sub>SO<sub>4</sub>) using the Ti/β-PbO<sub>2</sub>/PTFE anode prepared with  $VR_{PTFE} = 6$  mL L<sup>-1</sup>; a blank CV for 0.1 mol L<sup>-1</sup> Na<sub>2</sub>SO<sub>4</sub> is also shown. For electrode potentials ( $E$ ) < 1.7 V, two current peaks related to NOR electrooxidation can be identified (at about 1.2 and 1.5 V). Then, for  $E > 1.7$  V, the current density ( $j$ ) values increase significantly due to the oxygen evolution reaction (OER); despite the decrease in those  $j$  values from the first

to the fifth scan, they are greater than the ones for the blank CV. Thus, it can be inferred that NOR oxidation is occurring simultaneously with the OER, i.e. there is no passivation of the anode. In the reverse scan, only one reduction peak is present (at  $E$  slightly more positive than 1.0 V), which can be associated to the oxidation peak at ~1.2 V. Here it is interesting to compare the blank CV obtained using the Ti/β-PbO<sub>2</sub>/PTFE anode with the one obtained using a Si/BDD anode (500 ppm B doping; purchased from NeoCoat, Switzerland) – see **Fig. 5**. Despite the hydrophobic nature of the surface of the Ti/β-PbO<sub>2</sub>/PTFE anode (see section 3.1), the OER overpotential for this anode is significantly less positive (~500 mV) than the one for the Si/BDD anode; clearly, the increased surface hydrophobicity of the Ti/β-PbO<sub>2</sub>/PTFE anode does not contribute to increase its oxidation power, contrary to what was claimed by Zhao et al. [35].

### 3.3. Effect of operational variables on the electrochemical degradation of NOR

Firstly, the possible effect of solution pH on the NOR electrodegradation using the Ti/ $\beta$ -PbO<sub>2</sub>/PTFE anode was assessed (at  $j = 20 \text{ mA cm}^{-2}$ ). As can be seen in Fig. 6a, which shows the evolution of the remaining fraction of NOR ( $x_{\text{NOR}}^{\text{rem}}$ ) as a function of the applied electric charge per unit volume of electrolyzed solution ( $Q_{\text{ap}}$ ) for solutions of pH = 3, 7, and 10 (or with no pH control), similar  $x_{\text{NOR}}^{\text{rem}}$  decay profiles were obtained. Hence, no significant differences were observed in the obtained removal rates ( $k_{1\text{st}} \approx 1.4 \times 10^{-2} \text{ min}^{-1}$ , as can be seen in simply Tables SC–1 in the supplementary content file) despite the fact that NOR has two distinct  $\text{pK}_a$  values (at 6.34 for the carboxylic group and at 8.75 for the nitrogen of the piperazinyl group). This suggests that the NOR chemical form (ionic or molecular) plays no significant role on the oxidation mechanism. Consequently, in principle the electro-oxidation process is expected to depend only on the transport of the NOR molecule from the solution bulk to a region close to the anode surface, i.e. to be mass transport controlled. Then the  $x_{\text{NOR}}^{\text{rem}}$  decay should be that of the theoretical exponential line of a process purely controlled by mass transport, estimated as:

$$x_{\text{NOR}}^{\text{rem}} = \frac{[\text{NOR}]_t}{[\text{NOR}]_0} = \exp\left(-\frac{Ak_m t}{V}\right) \quad (7)$$

where  $A$  is the geometric area ( $\text{m}^2$ ) of the working electrode,  $k_m$  the mass transfer coefficient ( $\text{m s}^{-1}$ ), and  $V$  the electrolyzed solution volume ( $\text{m}^3$ ). The  $k_m$  value was obtained after determining: a) the thickness of the stagnant layer ( $2.16 \times 10^{-5} \text{ m}$ ) through a simple electrochemical assay based on the  $[\text{Fe}(\text{CN})_6]^{3-/4-}$  redox couple [45]; b) the NOR diffusion coefficient ( $5.65 \times 10^{-10} \text{ m}^2 \text{ s}^{-1}$ ) using a diaphragm cell [46]. The faster empirical decay of  $x_{\text{NOR}}^{\text{rem}}$  comparatively to that theoretically predicted (see Fig. 6a) is probably related to indirect oxidation processes in the solution bulk mediated by electrogenerated oxidants such as  $\text{H}_2\text{O}_2$  [47], which was indeed detected in the electrolyzed solution and presented a decreased concentration in the presence of NOR (see Fig. SC–3 in the

supplementary content file), or to an increased  $k_m$  value attained because of the extra turbulence brought on by the parasitic OER, as reported by Flox et al. [48].

Secondly, the possible effect of  $j$  on the NOR electrodegradation using the Ti/ $\beta$ -PbO<sub>2</sub>/PTFE anode was assessed (with no pH control). Fig. 6b shows the evolution of  $x_{\text{NOR}}^{\text{rem}}$  as a function of  $Q_{\text{ap}}$  for different values of  $j$  (10, 20, and 30  $\text{mA cm}^{-2}$ ); again, similar  $x_{\text{NOR}}^{\text{rem}}$  decay profiles were obtained. Thus, as the electrochemical system is under mass transfer limitations (exponential decay), the use of low current density values is recommended; however, as shown in simply Tables SC–1 in the supplementary content file, the NOR removal rate progressively increases with  $j$ . At this point, it is possible to estimate the initial limiting current density ( $j_{\text{lim}}^0$ ), i.e. the maximum rate at which NOR can be oxidized on the surface of the Ti/ $\beta$ -PbO<sub>2</sub>/PTFE anode, using the following equation:

$$j_{\text{lim}}^0 = nFk_m[\text{NOR}]_0 \quad (8)$$

where  $n$  is the number of electrons involved in the degradation process (see eq. (3)) and  $[\text{NOR}]_0 = 0.313 \text{ mol m}^{-3}$ . The obtained value of  $j_{\text{lim}}^0$  is  $\sim 7 \text{ mA cm}^{-2}$ ; thus, the proximity of the empirical decay of  $x_{\text{NOR}}^{\text{rem}}$  at 10  $\text{mA cm}^{-2}$  (the lowest investigated  $j$  value) comparatively to that theoretically predicted (see Fig. 6b). In principle, any further increase in the  $j$  value leads only to an increased OER. However, once again it is important to highlight the possible electrogeneration of oxidants at higher  $j$  values, such as  $\text{O}_3$  and  $\text{H}_2\text{O}_2$  [47], or the improved mass transfer conditions attained because of an increased OER [48]. These aspects are possibly responsible for the higher empirical NOR removal rates obtained at  $j = 20$  and 30  $\text{mA cm}^{-2}$  (see simply Tables SC–1 in the supplementary content file) comparatively to the theoretical data (based on a purely mass transfer-controlled process).

Thirdly, the possible effect of solution temperature on the NOR electrodegradation using the Ti/ $\beta$ -PbO<sub>2</sub>/PTFE anode was assessed (at  $j = 20 \text{ mA cm}^{-2}$  and with no pH control). Fig. 7a shows the evolution of  $x_{\text{NOR}}^{\text{rem}}$  as a function of  $Q_{\text{ap}}$  for the different temperatures (10, 25, and 40 °C). As can be inferred from the pseudo-first order kinetic constants listed in simply Tables SC–1 in the supplementary

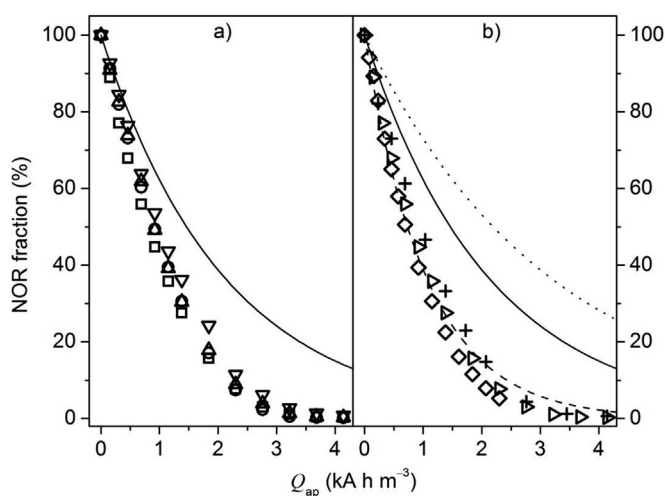


**Fig. 6.** NOR fraction remaining in solution as a function of the applied charge per unit volume of this solution ( $Q_{\text{ap}}$ ) for electrolyses carried out using the Ti/ $\beta$ -PbO<sub>2</sub>/PTFE anode (prepared with  $\text{VR}_{\text{PTFE}} = 6 \text{ mL L}^{-1}$ ) and distinct: **a)** solution pH values (3 (○), 7 (△), 10 (▽), and no pH control (□)); **b)** current density values (10 (◇), 20 (▷), and 30  $\text{mA cm}^{-2}$  (+)). Theoretical line based on a system controlled by mass transport for 10 (---), 20 (—), and 30 (...)  $\text{mA cm}^{-2}$ . The electrolysis conditions were set at 25 °C, using 20  $\text{mA cm}^{-2}$  for **a)** and no pH control for **b)**.

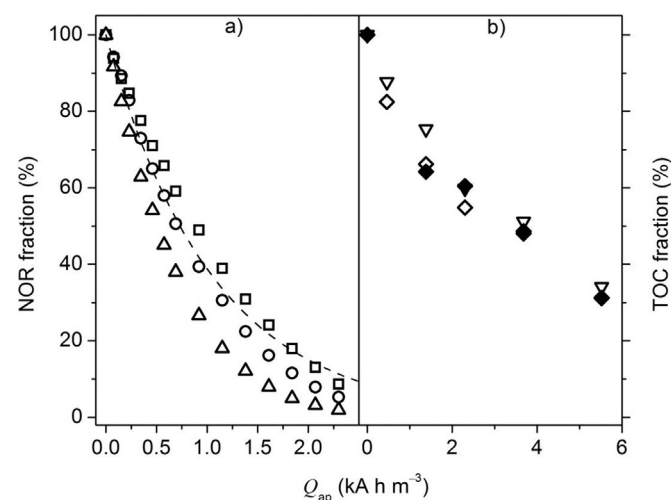


**Fig. 7.** **a)** NOR fraction remaining in solution vs.  $Q_{\text{ap}}$  for electrolyses carried out at distinct temperatures (10 (□), 25 (○), and 40 (△) °C)\*; **b)** TOC fraction remaining in solution vs.  $Q_{\text{ap}}$  for electrolyses carried out at the optimized condition\*\* with the Ti/ $\beta$ -PbO<sub>2</sub>/PTFE anode (<math>\diamond/\blacklozenge</math>: replicate experiments) or a Ti-Pt/ $\beta$ -PbO<sub>2</sub> anode (▽) obtained using an electrodeposition bath with sodium dodecyl sulfate (SDS) as additive (no PTFE present). Ti/ $\beta$ -PbO<sub>2</sub>/PTFE anode prepared with  $\text{VR}_{\text{PTFE}} = 6 \text{ mL L}^{-1}$ . \* 20  $\text{mA cm}^{-2}$  (no pH control); \*\* 10  $\text{mA cm}^{-2}$  at 40 °C (no pH control).

content file, the NOR removal rate increased slightly with temperature (mainly at 40 °C) due to a gradual increase in the NOR diffusion coefficient; the possible increase of the oxidation power of electrogenerated oxidants (chemical oxidation), or even of their concentration, might also have a positive effect on the NOR removal rate.

Next, the capability of the Ti/ $\beta$ -PbO<sub>2</sub>/PTFE anode to mineralize NOR and its degradation intermediates was assessed by TOC measurements under the optimized operational conditions ( $j = 10 \text{ mA cm}^{-2}$ , no pH control, and 40 °C) – see Fig. 7b. As expected for oxide based anodes, the conversion rate of NOR to CO<sub>2</sub> ( $\sim 1.5 \times 10^{-3} \text{ min}^{-1}$ , which is similar to the one attained with a Ti-Pt/ $\beta$ -PbO<sub>2</sub> anode prepared using only SDS as additive [25] – see Fig. 7b) is significantly lower than the NOR removal rate, since several hydroxylation reactions must occur on the anode surface for the attainment of total mineralization of the NOR load. Consequently, as can be seen in Fig. SC–4 in the supplementary content file, the mineralization current efficiency (MCE) was somewhat low (close to 30%) in the first stages of the electrooxidation process and decreased to smaller values as the organic load was gradually converted to CO<sub>2</sub>; for a TOC removal of 70% after 12 h of electrolysis, the energy consumption per unit mass of removed TOC ( $w$ ) was

$\sim 2 \text{ kW h g}^{-1}$ . When these values are compared to those attained for the electrochemical degradation of NOR using distinct Si/BDD anodes under the same experimental conditions [37], the latter anodes stand out since MCE values close to 60% were attained in the initial stages of the NOR mineralization process, with average  $w$  values of  $5 \text{ kW h g}^{-1}$  for a TOC removal of 90% after only 5 h of electrolysis. In fact, the attained extent of electrochemical combustion ( $\varphi$ ) of the removed NOR was  $\sim 70\%$  after 12 h of electrolysis using the Ti/ $\beta$ -PbO<sub>2</sub>/PTFE anode, in comparison to  $\sim 80\%$  after only 5 h of electrolysis using the distinct Si/BDD anodes [37]; these results confirm that, contrary to what was claimed by Zhao et al. [35], the oxidation capability (oxidation power) of the PTFE-doped  $\beta$ -PbO<sub>2</sub> anode is lower than that of Si/BDD anodes, as could be inferred from a comparison of the OER onset potentials for these anodes (see section 3.2 above).

Considering that there is no significant contribution from electrogenerated oxidant-mediated chemical oxidation to the organic load mineralization, the NOR degradation using the Ti/ $\beta$ -PbO<sub>2</sub>/PTFE anode is expected to occur with significant accumulation of degradation intermediates. Consequently, LC-MS/MS analyses were carried out to determine the main initial degradation intermediates resulting from the NOR oxidation – see Table 1; the proposed

**Table 1**  
LC-MS/MS data for the intermediate compounds detected during the electrooxidation of norfloxacin using the Ti/ $\beta$ -PbO<sub>2</sub>/PTFE anode.<sup>a</sup>

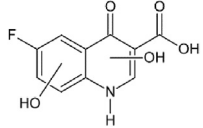
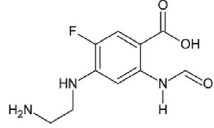
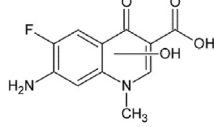
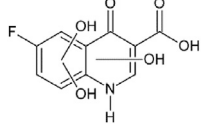
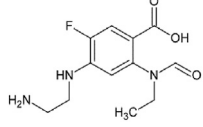
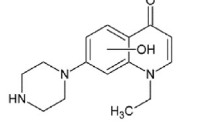
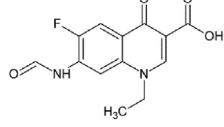
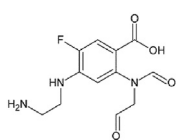
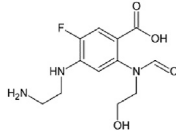
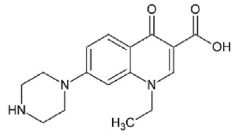
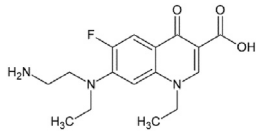
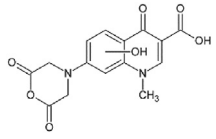
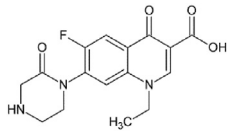
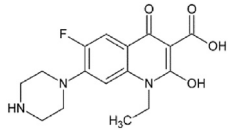
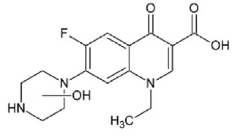
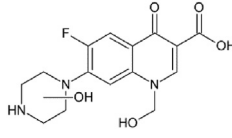
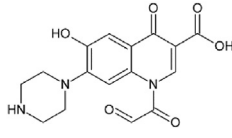
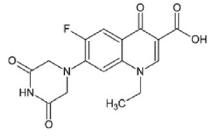
Molecular mass (Da)	Retention time (min)	Molecular ion [M+H] <sup>+</sup> ( $m/z$ )	Main fragment ions ( $m/z$ )	Proposed chemical structure
239	5.01	240	222, 176, and 166	
241	9.39	242	214, 198, 159, and 132	
252(a)	8.05	253	225, 209, 191, 179, and 163	
252(b)	6.31	253	209	
255(a)	2.52	256	238, 220, 212, 194, and 122	
255(b)	2.66	256	212	
255(c)	6.38	256	212	
269	9.36	270	242, 214, 198, and 186	
273	9.16	274	245, 216, 190, and 161	
278	8.35	279	261, 233, and 205	

Table 1 (continued)

Molecular mass (Da)	Retention time (min)	Molecular ion $[M+H]^+$ ( $m/z$ )	Main fragment ions ( $m/z$ )	Proposed chemical structure
283	7.33	284	266, 252, and 206	
285	8.59	286	268, 240, and 228	
301	7.49	302	282, 258, and 231	
321	5.43	322	304, 284, 276, and 233	
332	5.12	333	289, 275, and 231	
333	6.20	334	316, 290, 233, 205, and 176	
335(a)	6.43	336	318, 292, and 275	
335(b)	9.95	336	290, 276, and 262	
337	7.45	338	320, 302, 232, and 177	
345	9.10	346	328, 299, and 270	
347	6.66	348	330, 304, 256, and 217	

<sup>a</sup> Electrolysis conditions: 10 mA cm<sup>-2</sup> at 40 °C (no pH control).



fragmentation routes for the main detected initial degradation intermediates can be seen in Figs. SC–5 to SC–19 in the supplementary content file. As can be inferred from the data in Table 1, the detected initial degradation intermediates resulted from four main oxidation pathways due to the presence of many reactive sites in the NOR molecule: i) hydroxylation and/or oxidation reactions in the fluoroquinolone structure, ii) removal or hydroxylation of the piperazinyl group, iii) hydroxylated defluorination, and iv) removal or hydroxylation/oxidation of the ethyl group. These oxidation pathways were also observed for the degradation of other fluoroquinolone antibiotics by HO $\cdot$  attack [49,50]. Hydroxylation reactions of the piperazinyl group (see compounds with  $m/z$  332, 333, 335(b), 337, and 347) followed by ring opening, dealkylation, and deamination processes (see compounds with  $m/z$  241, 269, 283, and 285) seem to be predominant during the NOR electrooxidation using the Ti/ $\beta$ -PbO $_2$ /PTFE or Si/BDD (see Ref. [37]) anodes. The mechanism of hydroxylation of the piperazinyl group and subsequent ring opening is similar to the one described by Jiang et al. [51] for the sulfate radical-based oxidation of ciprofloxacin. Similar results have been reported on the susceptibility of the piperazinyl group of other fluoroquinolone antibiotics to oxidation by different routes: TiO $_2$  heterogeneous catalysis [49], ozonation [52], photolysis [53], Fenton reaction [54], and even biodegradation [55]. That behavior might be due to the combination of the lone pair electrons of N and the electrophilic nature of HO $\cdot$ , which can rapidly react by hydrogen atom abstraction or addition [56]. Other initial degradation intermediates were detected during the NOR electrooxidation using the Ti/ $\beta$ -PbO $_2$ /PTFE anode, but the peak intensity was not high enough to render their MS/MS analysis possible. The number of detected initial degradation intermediates for the NOR electrooxidation using the Ti/ $\beta$ -PbO $_2$ /PTFE anode is significantly greater than the one detected using Si/BDD anodes at varying boron doping levels [37], confirming the lower oxidation capability of the former anode, contrary to what was initially expected. Thus, the PTFE-doping of the  $\beta$ -PbO $_2$  film only led to a stabler anode material, with a significantly longer service life (see section 3.1 above). In fact, only one Ti/ $\beta$ -PbO $_2$ /PTFE anode (prepared with  $V_{R_{PTFE}} = 6 \text{ mL L}^{-1}$ ) was used for all the NOR electrochemical degradation experiments in this work (more than 300 h of operation at 10–20 mA cm $^{-2}$ ), without any significant leaching of Pb $^{2+}$  ions to the electrolyzed solutions (only two experimental conditions resulted in [Pb $^{2+}$ ] values around 0.3 mg L $^{-1}$ ).

Terminal degradation intermediates (short-chain carboxylic acids), resulting from the opening and further oxidation of the fluoroquinolone structure and the piperazine ring, were also detected (by HPLC). Among them, six acids (from C1 to C4: formic, oxalic, glycolic, oxamic, propionic, and malic acids) were identified and the evolution of their concentration throughout the electrolysis was determined (see Fig. 8). After 7 h of electrolysis, the highest concentrations were those for glycolic, propionic, and malic acids, with the concentration of malic acid already decreasing whereas those of the other two acids were still increasing, accumulating in the electrolyzed solution. The recalcitrant oxalic and oxamic acid were only detected at low and very low concentrations, respectively. The total concentration of carbon ( $\sim 20 \text{ mg L}^{-1}$ ) contained within the six identified carboxylic acids after 7 h of electrolysis ( $Q_{ap} \approx 3.2 \text{ kA h m}^{-3}$ ) corresponds to approximately 2/3 of the remaining TOC fraction – see Fig. 7b.

Finally, the antibacterial activity against *E. coli* of the electrolyzed NOR solution was determined as a function of the electrolysis time,  $t$ . Thus, the evolution of the corresponding *E. coli* inhibition index with  $t$  is shown in Fig. 9 (along with [NOR] vs.  $t$ ). As reported by Domagala [57], the antibacterial efficacy of quinolone based antibiotics is dictated by its substituents, mainly the presence of halogen atoms and the piperazine ring. Clearly, the antibacterial

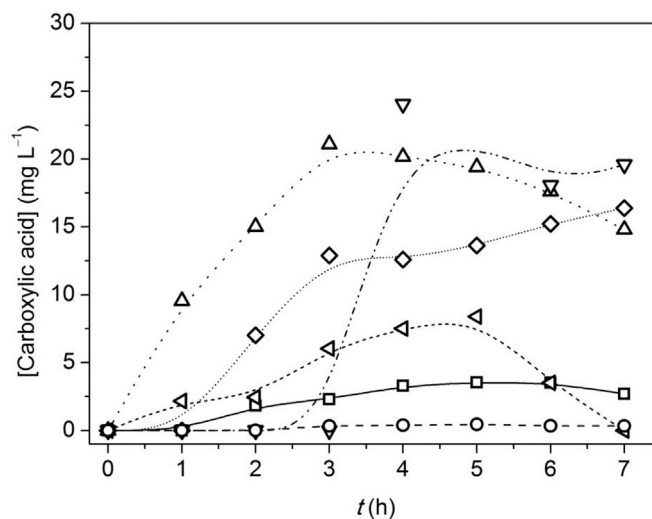


Fig. 8. Evolution of the concentration of the six identified short-carboxylic acids as a function of electrolysis time using the Ti/ $\beta$ -PbO $_2$ /PTFE anode prepared with  $V_{R_{PTFE}} = 6 \text{ mL L}^{-1}$ : oxalic ( $\square$ ), oxamic ( $\circ$ ), malic ( $\triangle$ ), glycolic ( $\nabla$ ), formic ( $\triangleleft$ ), and propionic ( $\diamond$ ) acids. Electrolysis conditions: 10 mA cm $^{-2}$  at 40 °C (no pH control). The lines were plotted using a spline function within the Origin $^{\text{®}}$  software.

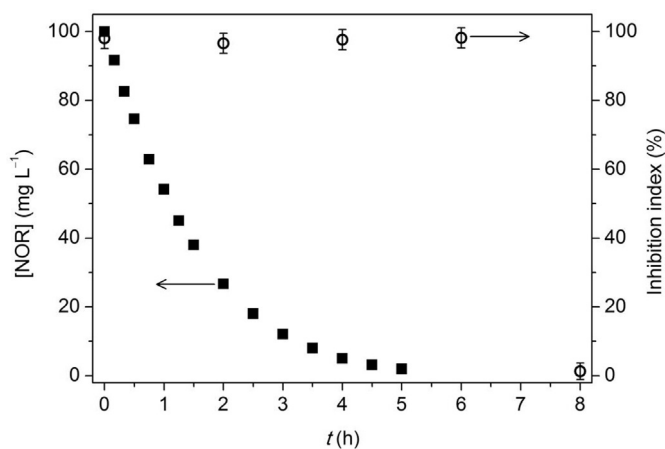


Fig. 9. Evolution of [NOR] ( $\blacksquare$ ) and the *E. coli* inhibition index ( $\circ$ ) as a function of electrolysis time using the Ti/ $\beta$ -PbO $_2$ /PTFE anode prepared with  $V_{R_{PTFE}} = 6 \text{ mL L}^{-1}$ . The error bars refer to the calculated errors for triplicate analyses. Electrolysis conditions: 10 mA cm $^{-2}$  at 40 °C (no pH control).

activity of the electrolyzed solution was not yet eliminated when almost complete removal of NOR was achieved. This might be due to the combination of the low minimum inhibitory value of [NOR] ( $< 1 \text{ mg L}^{-1}$  [58], not detectable by the HPLC experiments performed in this work) and the soft oxidation prompted by the Ti/ $\beta$ -PbO $_2$ /PTFE anode that results in hydroxylated intermediates with an intact fluoroquinolone structure, as reported by Sturini et al. [59] when investigating the photodegradation of six fluoroquinolones. This reasoning is corroborated by the relatively low levels of TOC removal ( $\sim 40$  and  $\sim 50\%$  after 5 and 8 h of electrolysis, respectively) and the significant number of initial intermediates detected (see Table 1). Nevertheless, it should be noted that Wammer et al. [60], who investigated the direct aquatic photochemistry of NOR (for [NOR] $_0 = 31.9 \text{ mg L}^{-1}$ ), reported antibacterial activity against *E. coli* only by NOR itself and not by its photodegradation products. When the electrodegradation of NOR was carried out using a Si/BDD anode [37], the inhibition index fell to zero concomitantly with the

attainment of total removal of NOR (after about 5 h of electrolysis); in that case, the mineralization of the produced intermediates was high (90% TOC removal after 5 h of electrolysis [37]). As previously pointed out [37], short-chain carboxylic acids do not inhibit the growth of *E. coli*, at least in the range of concentrations measured in this work.

#### 4. Conclusions

The electrodeposited PTFE-doped PbO<sub>2</sub> films exhibited the desired  $\beta$  phase, the characteristic tetragonal crystallites, and a high degree of hydrophobicity due to PTFE co-deposition with the  $\beta$ -PbO<sub>2</sub> crystallites. These films led to Ti/ $\beta$ -PbO<sub>2</sub>/PTFE anodes with improved electrochemical stability, presenting significantly longer service lives (considering Ti substrate passivation, comparatively to a non-PTFE-doped Ti/ $\beta$ -PbO<sub>2</sub> anode) and low (if detectable) leaching of Pb<sup>2+</sup> ions. Nevertheless, the oxygen evolution reaction overpotential for an optimized Ti/ $\beta$ -PbO<sub>2</sub>/PTFE anode was significantly less positive (~500 mV) than the one for a Si/BDD anode, contrary to what has been reported by Zhao et al. [35]. Hence, despite the observed capability of the optimized Ti/ $\beta$ -PbO<sub>2</sub>/PTFE anode to oxidize NOR, which was successfully achieved applying 10 mA cm<sup>-2</sup> at 40 °C (independently of the solution pH), the attained mineralization rate and level were low in comparison to those attained when Si/BDD anodes were used. In addition, low values of mineralization current efficiency and extent of total electrochemical combustion were attained. Consequently, a high number of aromatic intermediates was observed, resulting from hydroxylation and oxidation reactions in the fluoroquinolone structure as well as on its substituents (mainly in the piperazine ring). Some of these degradation intermediates seem to inhibit the growth of *E. coli*, as the antibacterial activity of the electrolyzed solution is not yet eliminated when almost complete removal of NOR is achieved; the antibacterial activity was eliminated only after a longer electrolysis time, probably due to the attainment of complete degradation of the fluoroquinolone structure. In summary, the doping of the  $\beta$ -PbO<sub>2</sub> film with PTFE led to an anode with a significantly improved service life, but its oxidation capability (medium oxidation power, characteristic of metal oxide anodes) was not altered, contrary to what has been reported in the literature [35].

#### Acknowledgments

Financial support and scholarships from the Brazilian funding agencies FAPESP (São Paulo Research Foundation, grant numbers 2008/10449-7, 2012/13587-7, and 2014/11597-0) and CNPq (National Council of Scientific and Technological Development, grant number 487270/2012-6) are gratefully acknowledged. Professor Edenir Rodrigues Pereira Filho (DQ-UFSCar) is acknowledged for the AAS analyses. The supply of NOR and PTFE-dispersion samples by Vita Nova and DuPont Brasil, respectively, is also gratefully acknowledged.

#### Appendix A. Supplementary data

Supplementary data related to this article can be found at <https://doi.org/10.1016/j.electacta.2018.07.122>.

#### References

- [1] C. Postigo, D. Barceló, Synthetic organic compounds and their transformation products in groundwater: occurrence, fate and mitigation, *Sci. Total Environ.* 503–504 (2015) 32–47.
- [2] M.D. Hernandez, M. Mezcuá, A.R. Fernández-Alba, D. Barceló, Environmental risk assessment of pharmaceutical residues in wastewater effluents, surface waters and sediments, *Talanta* 69 (2006) 334–342.
- [3] P. Norberg, D.M. Monnet, O. Cars, Antibacterial Drug Resistance (Background Document for the WHO Project: Priority Medicines for Europe and the World), World Health Organization, Geneva, 2005.
- [4] J. Wang, S. Wang, Removal of pharmaceuticals and personal care products (PPCPs) from wastewater: a review, *J. Environ. Manag.* 182 (2016) 620–640.
- [5] K.G. Karthikeyan, M.T. Meyer, Occurrence of antibiotics in wastewater treatment facilities in Wisconsin, USA, *Sci. Total Environ.* 361 (2006) 196–207.
- [6] X. Van Doorslaer, J. Dewulf, H. Van Langenhove, K. Demeestere, Fluoroquinolone antibiotics: an emerging class of environmental micropollutants, *Sci. Total Environ.* 500–501 (2014) 250–269.
- [7] A.J. Watkinson, E.J. Murby, D.W. Kolpin, S.D. Costanzo, The occurrence of antibiotics in an urban watershed: from wastewater to drinking water, *Sci. Total Environ.* 407 (2009) 2711–2723.
- [8] G. Mamba, A.K. Mishra, Graphitic carbon nitride (g-C<sub>3</sub>N<sub>4</sub>) nanocomposites: a new and exciting generation of visible light driven photocatalysts for environmental pollution remediation, *Appl. Catal., B* 198 (2016) 347–377.
- [9] M. Zalfani, B. van der Schueren, M. Mahdouani, R. Bourguiga, W.-B. Yu, M. Wu, O. Deparis, Y. Li, B.-L. Su, ZnO quantum dots decorated 3DOM TiO<sub>2</sub> nanocomposites: symbiose of quantum size effects and photonic structure for highly enhanced photocatalytic degradation of organic pollutants, *Appl. Catal., B* 199 (2016) 187–198.
- [10] Z. Wang, M. Xu, F. Wang, X. Liang, Y. Wei, Y. Hu, C.G. Zhu, W. Fang, Preparation and characterization of a novel Ce doped PbO<sub>2</sub> electrode based on NiO modified Ti/TiO<sub>2</sub>NTs substrate for the electrocatalytic degradation of phenol wastewater, *Electrochim. Acta* 247 (2017) 535–547.
- [11] I. Oller, S. Malato, J.A. Sánchez-Pérez, Combination of advanced oxidation processes and biological treatments for wastewater decontamination - a review, *Sci. Total Environ.* 409 (2011) 4141–4166.
- [12] F. Meng, G. Fu, D. Butler, Water quality permitting: from end-of-pipe to operational strategies, *Water Res.* 101 (2016) 114–126.
- [13] E. Brillas, C.A. Martínez-Huitle, Decontamination of wastewaters containing synthetic organic dyes by electrochemical methods. An updated review, *Appl. Catal., B* 166–167 (2015) 603–643.
- [14] C.A. Martínez-Huitle, M.A. Rodrigo, I. Sirés, O. Scialdone, Single and coupled electrochemical processes and reactors for the abatement of organic water pollutants: a critical review, *Chem. Rev.* 115 (2015) 13362–13407.
- [15] M. Panizza, G. Cerisola, Application of diamond electrodes to electrochemical processes, *Electrochim. Acta* 51 (2005) 191–199.
- [16] A. Kapalka, G. Fóti, C. Comninellis, The importance of electrode material in environmental electrochemistry: formation and reactivity of free hydroxyl radicals on boron-doped diamond electrodes, *Electrochim. Acta* 54 (2009) 2018–2023.
- [17] A. Kapalka, G. Fóti, C. Comninellis, Kinetic modelling of the electrochemical mineralization of organic pollutants for wastewater treatment, *J. Appl. Electrochem.* 38 (2008) 7–16.
- [18] D. Shao, X. Li, H. Xu, W. Yan, An improved stable Ti/Sb–SnO<sub>2</sub> electrode with high performance in electrochemical oxidation processes, *RSC Adv.* 4 (2014) 21230–21237.
- [19] M. Xu, Z. Wang, F. Wang, P. Hong, C. Wang, X. Ouyang, C. Zhu, Y. Wei, Y. Hun, W. Fang, Fabrication of cerium doped Ti/nano TiO<sub>2</sub>/PbO<sub>2</sub> electrode with improved electrocatalytic activity and its application in organic degradation, *Electrochim. Acta* 201 (2016) 240–250.
- [20] H. Lin, J. Niu, J. Xu, H. Huang, D. Li, Z. Yue, C. Feng, Highly efficient and mild electrochemical mineralization of long-chain perfluorocarboxylic acids (C<sub>9</sub>–C<sub>10</sub>) by Ti/SnO<sub>2</sub>–Sb–Ce, Ti/SnO<sub>2</sub>–Sb/Ce–PbO<sub>2</sub>, and Ti/BDD electrodes, *Environ. Sci. Technol.* 47 (2013) 13039–13046.
- [21] Q. Qiao, S. Singh, S.-L. Lo, Y. Lim, J. Jin, L. Wang, Electrochemical oxidation of acid orange 7 dye with Ce, Nd, and Co-modified PbO<sub>2</sub> electrodes: preparation, characterization, optimization, and mineralization, *J. Taiwan Inst. Chem. Eng.* 84 (2018) 110–122.
- [22] K. Zhou, Y. Tian, H. Ma, C. Ma, Y. Fu, X. Dong, X. Zhang, Photoelectrocatalytic performance of conductive carbon black-modified Ti/F-PbO<sub>2</sub> anode for degradation of dye wastewater (reactive brilliant blue KN-R), *J. Solid State Electrochem.* 22 (2018) 1131–1142.
- [23] X. Li, H. Xu, W. Yan, Fabrication and characterization of PbO<sub>2</sub> electrode modified with polyvinylidene fluoride (PVDF), *Appl. Surf. Sci.* 389 (2016) 278–286.
- [24] Q. Zhuo, Q. Xiang, H. Yi, Z. Zhang, B. Yang, K. Cui, X. Bing, Z. Xu, X. Liang, Q. Guo, R. Yang, Electrochemical oxidation of PFOA in aqueous solution using highly hydrophobic modified PbO<sub>2</sub> electrodes, *J. Electroanal. Chem.* 801 (2017) 235–243.
- [25] J.M. Aquino, K. Irikura, R.C. Rocha-Filho, N. Bocchi, S.R. Biaggio, A comparison of electrodeposited Ti/ $\beta$ -PbO<sub>2</sub> and Ti-Pt/ $\beta$ -PbO<sub>2</sub> anodes in the electrochemical degradation of the Direct Yellow 86 dye, *Quim. Nova* 33 (2010) 2124–2129.
- [26] M.J. Nunes, N. Monteiro, M.J. Pacheco, A. Lopes, L. Ciriaco, Ti/ $\beta$ -PbO<sub>2</sub> versus Ti/Pt/ $\beta$ -PbO<sub>2</sub>: influence of the platinum interlayer on the electrodegradation of tetracyclines, *J. Environ. Sci. Health, Part A, Environ. Sci. Eng.* 51 (2016) 839–846.
- [27] W. Zhao, J. Xing, D. Chen, D. Jin, J. Shen, Electrochemical degradation of Musk ketone in aqueous solutions using a novel porous Ti/SnO<sub>2</sub>-Sb<sub>2</sub>O<sub>3</sub>/PbO<sub>2</sub> electrodes, *J. Electroanal. Chem.* 775 (2016) 179–188.
- [28] C. Wang, J. Niu, L. Yin, J. Huang, L.-A. Hou, Electrochemical degradation of fluoxetine on nanotube array intercalated anode with enhanced electronic transport and hydroxyl radical production, *Chem. Eng. J.* 346 (2018) 662–671.

- [29] G. Ramírez, F.J. Recio, P. Herrasti, C. Ponce-de-León, I. Sirés, Effect of RVC porosity on the performance of PbO<sub>2</sub> composite coatings with titanate nanotubes for the electrochemical oxidation of azo dyes, *Electrochim. Acta* 204 (2016) 9–17.
- [30] R.M. Farinos, L.A.M. Ruotolo, Comparison of the electrooxidation performance of three-dimensional RVC/PbO<sub>2</sub> and boron-doped diamond electrodes, *Electrochim. Acta* 224 (2017) 32–39.
- [31] S. Liu, Y. Wang, X. Zhou, W. Han, J. Li, X. Sun, J. Shen, L. Wang, Improved degradation of the aqueous flutriafol using a nanostructure macroporous PbO<sub>2</sub> as reactive electrochemical membrane, *Electrochim. Acta* 253 (2017) 357–367.
- [32] X. Duan, C. Zhao, W. Liu, X. Zhao, L. Chang, Fabrication of a novel PbO<sub>2</sub> electrode with a graphene nanosheet interlayer for electrochemical oxidation of 2-chlorophenol, *Electrochim. Acta* 240 (2017) 424–436.
- [33] X. Li, X. Li, W. Yang, X. Chen, W. Li, B. Luo, K. Wang, Preparation of 3D PbO<sub>2</sub> nanospheres@SnO<sub>2</sub> nanowires/Ti electrode and its application in methyl orange degradation, *Electrochim. Acta* 146 (2014) 15–22.
- [34] F.L. Souza, J.M. Aquino, K. Irikura, D.W. Miwa, M.A. Rodrigo, A.J. Motheo, Electrochemical degradation of the dimethyl phthalate ester on a fluorinated Ti/β-PbO<sub>2</sub> anode, *Chemosphere* 109 (2014) 187–194.
- [35] G. Zhao, Y. Zhang, Y. Lei, B. Lv, J. Gao, Y. Zhang, D. Li, Fabrication and electrochemical treatment application of a novel lead dioxide anode with superhydrophobic surfaces, high oxygen evolution potential, and oxidation capability, *Environ. Sci. Technol.* 44 (2010) 1754–1759.
- [36] X. Zhu, M. Tong, S. Shi, H. Zhao, J. Ni, Essential explanation of the strong mineralization performance of boron-doped diamond electrodes, *Environ. Sci. Technol.* 42 (2008) 4914–4920.
- [37] D.A.C. Coledam, J.M. Aquino, B.F. Silva, A.J. Silva, R.C. Rocha-Filho, Electrochemical mineralization of norfloxacin using distinct boron-doped diamond anodes in a filter-press reactor, with investigations of toxicity and oxidation by-products, *Electrochim. Acta* 213 (2016) 856–864.
- [38] J.M. Aquino, R.C. Rocha-Filho, N. Bocchi, S.R. Biaggio, Electrochemical degradation of the Reactive Red 141 dye on a b-PbO<sub>2</sub> anode assessed by the response surface methodology, *J. Braz. Chem. Soc.* 21 (2010) 324–330.
- [39] S. Silambarasan, A.S. Vangnai, Biodegradation of 4-nitroaniline by plant-growth promoting *Acinetobacter* sp. AVLB2 and toxicological analysis of its biodegradation metabolites, *J. Hazard. Mater.* 302 (2016) 426–436.
- [40] E. Brillas, I. Sirés, M.A. Oturan, Electro-Fenton process and related electrochemical technologies based on Fenton's reaction chemistry, *Chem. Rev.* 109 (2009) 6570–6631.
- [41] D.W. Miwa, G.R.P. Malpass, S.A.S. Machado, A.J. Motheo, Electrochemical degradation of carbaryl on oxide electrodes, *Water Res.* 40 (2006) 3281–3289.
- [42] G.F. Pereira, R.C. Rocha-Filho, N. Bocchi, S.R. Biaggio, Electrochemical degradation of the herbicide picloram using a filter-press flow reactor with a boron-doped diamond or β-PbO<sub>2</sub> anode, *Electrochim. Acta* 179 (2015) 588–598.
- [43] J. Feng, D.C. Johnson, Electrocatalysis of anodic oxygen-transfer reactions: titanium substrates for pure and doped lead dioxide films, *J. Electrochem. Soc.* 138 (1991) 3328–3337.
- [44] X. Chen, G. Chen, P.L. Yue, Stable Ti/IrOx-Sb<sub>2</sub>O<sub>5</sub>-SnO<sub>2</sub> anode for O<sub>2</sub> evolution with low Ir content, *J. Phys. Chem. B* 105 (2001) 4623–4628.
- [45] P. Cañizares, J. García-Gómez, I.F. de-Marcos, M.A. Rodrigo, J. Lobato, Measurement of mass-transfer coefficients by an electrochemical technique, *J. Chem. Educ.* 83 (2006) 1204–1207.
- [46] A.R. Gordon, The diaphragm cell method of measuring diffusion, *Ann. N. Y. Acad. Sci.* 46 (1945) 285–308.
- [47] M. Panizza, G. Cerisola, Direct and mediated anodic oxidation of organic pollutants, *Chem. Rev.* 109 (2009) 6541–6569.
- [48] C. Flox, E. Brillas, A. Savall, K. Groenen-Serrano, Kinetic study of the electrochemical mineralization of m-cresol on a boron-doped diamond anode, *Curr. Org. Chem.* 16 (2012) 1960–1966.
- [49] T. An, H. Yang, W. Song, G. Li, H. Luo, W.J. Cooper, Mechanistic considerations for the advanced oxidation treatment of fluoroquinolone pharmaceutical compounds using TiO<sub>2</sub> heterogeneous catalysis, *J. Phys. Chem. A* 114 (2010) 2569–2575.
- [50] L. Ge, G. Na, S. Zhang, K. Li, P. Zhang, H. Ren, Z. Yao, New insights into the aquatic photochemistry of fluoroquinolone antibiotics: direct photo-degradation, hydroxyl-radical oxidation, and antibacterial activity changes, *Sci. Total Environ.* 527–528 (2015) 12–17.
- [51] C. Jiang, Y. Ji, Y. Shi, J. Chen, T. Cai, Sulfate radical-based oxidation of fluoroquinolone antibiotics: kinetics, mechanisms and effects of natural water matrices, *Water Res.* 106 (2016) 507–517.
- [52] C. Liu, V. Nanaboina, G.V. Korshin, W. Jiang, Spectroscopic study of degradation products of ciprofloxacin, norfloxacin and lomefloxacin formed in ozonated wastewater, *Water Res.* 46 (2012) 5235–5246.
- [53] S. Babić, M. Periša, I. Škorić, Photolytic degradation of norfloxacin, enrofloxacin and ciprofloxacin in various aqueous media, *Chemosphere* 91 (2013) 1635–1642.
- [54] A.S. Giri, A.K. Golder, Ciprofloxacin degradation from aqueous solution by Fenton oxidation: reaction kinetics and degradation mechanisms, *RSC Adv.* 4 (2014) 6738–6745.
- [55] A. Prieto, M. Möder, R. Rodil, L. Adrian, E. Marco-Urrea, Degradation of the antibiotics norfloxacin and ciprofloxacin by a white-rot fungus and identification of degradation products, *Bioresour. Technol.* 102 (2011) 10987–10995.
- [56] P. Neta, R.E. Huie, A.B. Ross, Rate constants for reactions of inorganic radicals in aqueous solution, *J. Phys. Chem. Ref. Data* 17 (1988) 1027–1284.
- [57] J.M. Domagala, Structure-activity and structure-side-effect relationships for the quinolone antibacterials, *J. Antimicrob. Chemother.* 33 (1994) 685–706.
- [58] S.R. Norrby, M. Jonsson, Antibacterial activity of norfloxacin, *Antimicrob. Agents Chemother.* 23 (1983) 15–18.
- [59] M. Sturini, A. Speltini, F. Maraschi, L. Pretali, A. Profumo, E. Fasani, A. Albini, R. Migliavacca, E. Nucleo, Photodegradation of fluoroquinolones in surface water and antimicrobial activity of the photoproducts, *Water Res.* 46 (2012) 5575–5582.
- [60] K.H. Wammer, A.R. Korte, R.A. Lundeen, J.E. Sundberg, K. McNeill, W.A. Arnold, Direct photochemistry of three fluoroquinolone antibacterials: norfloxacin, ofloxacin, and enrofloxacin, *Water Res.* 47 (2013) 439–448.